Efficiency of different solar advanced oxidation processes on the oxidation of bisphenol A in water

Eva M. Rodríguez [a,*], Guadalupe Fernández [a], Nikolaus Klamerth [b], M. Ignacio Maldonado [b], Pedro M. Álvarez [a], Sixto Malato [b]

[a] *Departamento de Ingeniería Química y Química Física, Universidad de Extremadura, Avenida de Elvas s/n, 06071 Badajoz, Spain*
[b] *Plataforma Solar de Almería-CIEMAT, Ctra.de Senés s/n, 04200 Tabernas, Almería, Spain*

A R T I C L E   I N F O

A B S T R A C T

The efficiencies of different solar oxidation processes on the degradation of bisphenol A in water were studied. The work focuses on the removal and mineralization of bisphenol A and the formation of phenolic intermediates.

The processes tested were Fe(III) photolysis, ferricarboxylate photolysis, TiO_2 photocatalysis, H_2O_2 photolysis and combinations thereof. The influence of pH and the presence of hematite (α-Fe_2O_3) on their efficiency, as well as the nature of intermediates formed and development of toxicity were evaluated.

© 2010 Elsevier B.V. All rights reserved.

1. Introduction

Bisphenol A (BPA, 4,4′-dihydroxy-2,2-diphenylpropane) is used as an intermediate in the manufacture of polycarbonate, epoxy and polysulfonate resins. It has been demonstrated that BPA can alter the endocrine system, causing adverse effects in the reproductive systems of humans and animals and inducing the death of certain types of cells [1,2].

Numerous studies have confirmed its presence in rivers, in municipal wastewater treatment plant (MWWT) effluents and in sewage sludge. The concentration of BPA found in bodies of water (generally in the low μg L^{-1}), is several orders of magnitude below the chronic toxicity level, with the exception of streams polluted by industrial effluents [3]. Park and Choi [4], using *Daphnia magna* ecotoxicity tests, found the EC$_{50}$ of BPA to be 0.2 mg L^{-1}, and the LC$_{50}$ for the aquatic larva *Chironomus tentans* to be 3.3 mg L^{-1}.

Acute and chronic toxicity of BPA for other invertebrates and plants have recently been also compiled [5]. Elimination of BPA in water by biological processes [6], chemical oxidation [7,8] and advanced oxidation processes (AOPs) [9] has been studied in recent years. Regarding TiO$_2$ photocatalysis, Chiang et al. [10] observed that at pH 3, an aqueous solution of BPA (20 ppm) was completely mineralized after 120 min of UV illumination (20 W black light lamp with peak emission at 355 nm) in the presence of Degussa P25 TiO$_2$ particles. However, these authors also observed that toxic intermediates were generated during the early stage of BPA photodegradation at pH 3, as measured with the photoluminiscent bacteria *Vibrio fischeri*. Solar TiO$_2$ photocatalysis was studied by Kaneco et al. [11], who observed that BPA at a concentration of 10 mg L^{-1} in aqueous solution was completely mineralized at pH 6 and 30 °C after 11 h of exposure to sunlight in a slurry reactor loaded with 0.5 g L^{-1} of TiO$_2$ powder (99.9% anatase).

While the H$_2$O$_2$/UV combination was found effective for the elimination of BPA as well as deactivation of its estrogenic activity [12], the presence of Fe(II) (i.e., photo-Fenton system) enhanced the process efficiency [13]. Thus, a 9:0.9:1 H$_2$O$_2$:Fe(II):BPA ratio was enough for the complete removal of a concentration of 10 mg L^{-1} of BPA in less than 10 min of illumination (990W Xe lamp), while with a ratio of 90:9:1 more than 90% of BPA was converted into CO$_2$ after 36 h of irradiation. Application of UV-A light to a solution of BPA in simulated lake water was studied by Peng et al. [14], who observed that the presence of algae, humic acids and Fe(III) favoured the photodegradation of BPA. The positive effect of the presence of Fe(III) and humic acids in water was also observed in experiments using simulated sunlight [15].

In a study of combinations of Fe(III)/UV-A and ferrioxalate/UV-A, Zhou et al. observed that maximal efficiency of BPA degradation was obtained by the ferrioxalate/UV-A system at pH 3.5 with a

* Corresponding author. Tel.: +34 924289385; fax: +34 924289385.
E-mail address: evarguez@unex.es (E.M. Rodríguez).

ratio Fe(III):$C_2H_2O_4$ = 1:12 [16]. Under these conditions 24% mineralization was achieved after 160 min exposure to light compared to 7% without oxalate.

Regardless of the AOP applied, literature agrees on that the main degradation products of BPA come from the hydroxylation of the aromatic rings of BPA molecule, which evolve to quinones and further oxidize to aliphatic acids and eventually to CO_2 and inorganic ions [11,13,17]. According to Chiang et al. [10], some of the first intermediates are even more toxic than the parent compound.

In view of the comments above, the main purpose of this work was to study the efficiency of different solar AOPs for the degradation of bisphenol A in water, aimed at the intermediate generation and the removal of toxicity.

2. Experimental

2.1. Products, experimental set-up and procedure

Bisphenol A (99%, analytical grade) was supplied by Sigma–Aldrich. Other chemicals used were at least reagent grade and used as received. Distilled pilot plant feedwater was supplied by the Plataforma Solar de Almería distillation plant (conductivity < 10 $\mu S\,cm^{-1}$, Cl^- = 0.7–0.8 mg L^{-1}, NO_3^- = 0.5 mg L^{-1}, organic carbon < 0.5 mg L^{-1}).

Powdered P25 TiO_2 (surface area 51–55 $m^2\,g^{-1}$) was supplied directly by the manufacturer, Degussa AG (Frankfurt, Germany). Powdered natural red iron oxide (hematite) marketed as a pigment was obtained from Bendix, S.L (Spain).

Solar photocatalytic experiments were carried out in a 35-L pilot plant (24 L illuminated volume, 3.08 m^2 total irradiated surface) installed at the Plataforma Solar de Almería (PSA, latitude 37°N, longitude 2.4°W). A schematic of the plant can be seen in a previous publication [18]. It consists of two compound parabolic collectors (CPCs), a continuously stirred tank, a centrifugal recirculation pump (20 L min^{-1}) and connecting tubing and valves. Each CPC consists of a solar reflector (electropolished aluminium with a concentration factor of 1 and a radiation acceptance angle of 90°) and a tubular photoreactor made of borosilicate glass tubes (inner diameter 30.0 mm, outer diameter 31.8 mm, length 1.41 m, 12 tubes). The temperature inside the reactor was continuously recorded by a Pt-100 temperature probe. The global UV radiation (direct plus diffuse) was measured below 400 nm with a UV radiometer (CUV3 Model from KIPP&ZONEN).

To run the experiments the pilot plant was filled with 35 L of a 5×10^{-5} M BPA solution at pH 4–5 with the collectors covered. H_2SO_4 or NaOH (2 M) was added to the solution to reach the desired pH, and the solution was recirculated for 10 min through the whole system to ensure homogenisation. Then the chemicals for each experiment were added and the solution was homogenised for another 10 min. A sample was taken and analysed (t = 0), and the collectors were uncovered.

In Fenton and photo-Fenton systems, after pH adjustment, Fe(II) was added to the solution and homogenised, and finally H_2O_2 was added (t = 0) at the same time as the collectors were uncovered (photo-Fenton). Samples were taken at different times and analysed.

2.2. Analytical determinations.

Bisphenol A (BPA) concentration was determined by HPLC with an HPLC-DAD (Agilent Technologies, series 1100) system provided with a C-18 column (LUNA 5 mm, 3 mm × 150 mm, from Phenomenex) and using an acetonitrile–water (50/50, v/v) mixture as mobile phase (flow rate: 0.5 mL min^{-1}). Absorbance detection was made at 214 nm. Total organic carbon (TOC) was measured in filtered samples (Millipore-PVDF 0.45 μm filters) with a Shimadzu-5050A TOC analyser.

Samples for BPA and TOC analyses were mixed with $Na_2S_2O_3$ to ensure the destruction of any oxidizing agent remaining in solution.

Total dissolved iron concentration was determined by the ferrozine method which, briefly, consists of reduction to Fe(II) and further formation of a violet complex with the ferrozine reagent [19] (molar absorptivity at 565 nm: 27,044 $M^{-1}\,cm^{-1}$ [20]). The concentration of Fe(II) in solution was determined by the method of Zuo [21] with o-phenantroline by measuring complex absorbance at 510 nm (molar absorptivity: 11,040 $M^{-1}\,cm^{-1}$ [20]).

Total polyphenol concentration expressed as a BPA equivalent was determined by the Folin-Ciocalteau method [22]. The Folin-Ciocalteau reagent is a solution of complex polymeric ions formed from phosphomolybdic and phosphotungstic heteropoly acids. It oxidizes phenolates, reducing the heteropoly acids to a blue Mo–W complex that is measured at 740 nm (molar absorptivity for BPA: 9280 $M^{-1}\,cm^{-1}$). The procedure was as follows: 0.5 mL sample was added to a vial containing 0.5 mL reagent (Folin-Ciocalteau reagent) and 0.5 mL MilliQ water, and mixed for 3 min. Then 4 mL of Na_2CO_3 20% (w/v) were added, the sample was shaken, left for 1 h in darkness for the reaction and, finally, absorbance was measured at 740 nm. Since Fe(II) oxidized to Fe(III) by the Folin-Ciocalteau reagent may give a false positive, its contribution absorbance at 740 nm should be taken into account once Fe(II) concentration has been determined (molar absorptivity for Fe(II) by the Folin-Ciocalteau method: 1983 $M^{-1}\,cm^{-1}$). On the other hand, concentration of phenolic intermediates expressed as BPA equivalent can be calculated taking into account absorbance of the BPA and Fe(II) remaining in the samples at 740 nm.The hydrogen peroxide concentration was analysed spectrophotometrically by the ammonium metavanadate method based on absorbance at 450 nm (molar extinction coefficient: 283 $M^{-1}\,cm^{-1}$ [23]) of the red-orange peroxovanadium cation formed during the reaction of H_2O_2 with metavanadate.

Carboxylic acid concentrations were measured with a Dionex DX-600 ion chromatograph using a Dionex Ionpac AS11-HC 4 × 250 mm column and an ASRS 4 mm suppressor unit. The flow rate was 1.5 mL min^{-1} and elution was done with NaOH gradient programs.

Prior to GC–MS analysis of intermediates, the samples were preconcentrated by solid-phase extraction (SPE) using an extraction vacuum chamber (SUPELCO VISIPREP™) and 6 cm^3 OASIS(R) HLB cartridges. The cartridges were conditioned with 3 mL MeOH, 5 mL H_2O and 2 mL HCl (0.1N). After loading 250 mL of sample, the cartridges were washed with 5 mL MeOH 5%. Elution was carried out twice with 2.5 mL acetonitrile. Before elution, the cartridges were dried in nitrogen to ensure the total vaporization of water. The pH for the extraction was set close to 2 to ensure that acidic intermediates (like phenols) were uncharged, and therefore could be easily absorbed on the material of HLB cartridges [24]. After elution, the eluate was filtered (Millipore 0.45 μm PVDF filter).

GC–MS analyses were carried out with an Agilent Technologies HP 6890 series gas chromatograph equipped with an HP 5973 selective mass detector. Separation was performed with an HP-5HS capillary column (5% diphenyl/95% dimethylsiloxane), 30 m × 0.25 mm i.d., and 0.25 μm-thick film. A pulsed-splitless injector was used with a 10 μL injection volume, injector temperature of 250 °C, injection pulse pressure of 30 psi (2.5 min), and 8 psi inlet pressure. The helium flow rate was 50 mL min^{-1}, and column flow was 0.9 mL min^{-1}. The oven temperature program was 3 min at 70 °C, 10 °C/min up to 250 °C, hold at 250 °C for 2 min, 30 °C min^{-1} to 300 °C, and hold at 300 °C for 1.8 min, for a total run time of 26.5 min. Electron impact (EI with 70 eV) mass spectra were monitored from 40 to

Table 1
Advanced oxidation processes tested and experimental conditions applied. In all cases, $[BPA]_0 = 5 \times 10^{-5}$ M.

Run	pH	$[Fe(III)]_0$ 5×10^{-5} M	$[Fe(II)]_0$ 5×10^{-5} M	$[Oxalic]_0$ 10^{-3} M	$[Citric]_0$ 10^{-3} M	α-Fe$_2$O$_3$ 100 mg L^{-1}	TiO2 100 mg L^{-1}	$[H_2O_2]_0$ 10^{-3} M	Solar light
1	3	–	–	–	–	–	–	–	X
2	3	X	–	–	–	–	–	–	X
3	6.5	X	–	–	–	–	–	–	X
4	3	X	–	X	–	–	–	–	X
5	6.5	X	–	X	–	–	–	–	X
6	6.5	X	–	–	X	–	–	–	X
7	3	–	–	–	–	–	X	–	X
8	6.5	–	–	–	–	–	X	–	X
9	3	X	–	–	–	–	X	–	X
10	3	–	–	–	–	X	–	–	X
11	6.5	–	–	–	–	X	–	–	X
12	3	–	–	–	–	X	X	–	X
13	3	–	–	–	–	–	X	X	X
14	3	–	–	–	–	–	–	X	X
15	6.5	–	–	–	–	X	X	–	X
16	6.5	–	–	X	–	X	–	–	X
17	3	–	X	–	–	–	–	X	X
18	3	–	X	–	–	–	–	X	–

400 m/z. The ion source and quadrupole analyser temperatures were set at 230 °C.

A commercial assay marketed as Biofix® Lumi-10 was employed to evaluate the toxicity of samples towards a freeze-dried specially selected strain of the marine bacterium *V. fischeri* (NRRL number B-11177). Toxicity was evaluated in 1:1 diluted samples after adjusting the sample pH to 6–8. The drop in light emission of the bacteria after contact periods of 5, 15 and 30 min was measured and compared with a toxicant-free control (2% NaCl solution). Temperature was kept at 15 °C by a thermoblock and sample salinity was adjusted to 2%. When present in samples, hydrogen peroxide was removed after adjusting the pH and prior to toxicity analysis using catalase (catalase from bovine liver, 3390 units per mg of solid) acquired from Fluka Chemie AG (Buchs, Switzerland).

Textural characterization of commercial natural iron oxide was done by nitrogen adsorption at 77 K (Quantachrome Autosorb-1 automated gas adsorption system) and X-ray diffraction (XRD) (PW-1700 Philips diffractometer with Kα1 Cu radiation and recorded 2θ between 20° and 70°). A BET surface area of 23 m^2 g^{-1} and a total pore volume of 0.06 cm^3 g^{-1} were found. The XRD analysis confirmed the natural red iron oxide as hematite (α-Fe$_2$O$_3$) crystallites.

3. Results and discussion

Table 1 summarizes the conditions applied in the AOPs tested in this work.

3.1. BPA degradation

BPA degradation by the different processes and conditions shown in Table 1 was studied. Since this compound does not absorb radiation at wavelengths above 300 nm, exposure of BPA in water to sunlight (Run 1) did not cause any effect on BPA concentration. On the other hand, in those cases where BPA degradation was observed, BPA concentration followed first-order kinetics according to Eq. (1):

$$\ln\left(\frac{[BPA]}{[BPA]_0}\right) = -kt \tag{1}$$

where k (time^{-1}) is the pseudo-first-order rate constant. However, to compare the efficiency of the different solar oxidation processes

tested better, taking into consideration that the reaction time needed to degrade BPA also depends on the intensity of the incident UV radiation, BPA degradation is expressed as a function of the accumulated UV energy in the reactor, $Q_{UV,n}$:

$$\ln\left(\frac{[BPA]}{[BPA]_0}\right) = -k'Q_{UV,n} \tag{2}$$

where k' is the pseudo-first-order rate constant (L kJ^{-1}) and $Q_{UV,n}$ (kJ L^{-1}) the amount of accumulated UV energy received on any surface in the same position with regard to the sun, per unit of volume of water inside the reactor in the interval Δt. $Q_{UV,n}$ can be found by applying Eq. (3) [25]:

$$Q_{UV,n} = Q_{UV,n-1} + \Delta t_n \overline{UV}_{G,n} \frac{A_i}{V_T}; \quad \Delta t_n = t_n - t_{n-1} \tag{3}$$

where t_n is the time corresponding to n water sample, V_T total reactor volume (35 L), A_i illuminated surface area (3.08 m^2) and $\overline{UV}_{G,n}$ average solar ultraviolet radiation measured during the period Δt_n.
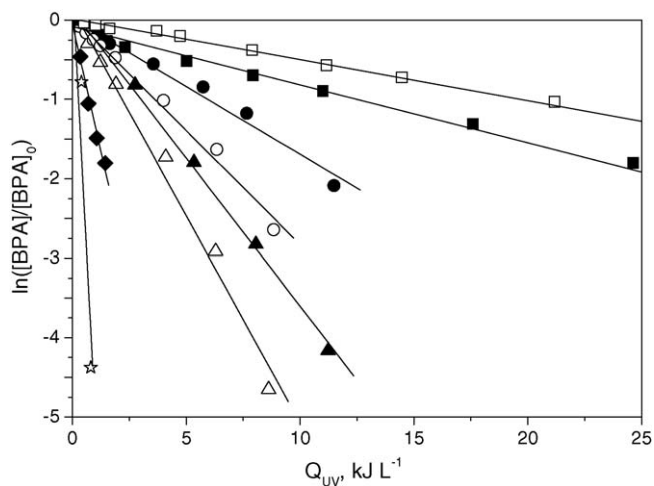

Fig. 1. Determination of BPA pseudo-first-order rate constant, k' (Eq. (2)). Experimental conditions in Table 1. Symbols: ■, Fe(III)/UV pH 3 (Run 2); ◆, Fe(III)/oxalic acid/UV pH 3 (Run 4); ●, TiO$_2$/UV pH 3 (Run 7); ○, TiO$_2$/UV pH 6.5 (Run 8); △, TiO$_2$/Fe(III) pH 3 (Run 9); ▲, TiO$_2$/α-Fe$_2$O$_3$/UV pH 3 (Run 12); □, α-Fe$_2$O$_3$/oxalic acid/UV pH 6.5 (Run 16); ☆, Fe(II)/H$_2$O$_2$/UV pH 3 (Run 17).

Fig. 1 shows the representation of the left-hand term of Eq. (2) against Q_{UV} for several selected runs. As it can be observed, points lie satisfactorily around straight lines in agreement with Eq. (2). Table 2 summarizes the calculated rate constants k' and the least-square correlation coefficients found from the linear regression analysis. The value of Q_{UV} needed to reduce initial BPA concentration by half ($Q_{UV,BPA(50)}$) was also determined for each oxidizing system using Eq. (4). Results are shown in Table 2.

$$Q_{UV,BPA(50)} = \frac{0.693}{k'} \text{ kJ L}^{-1} \quad (4)$$

Furthermore, by considering an average UV dose of 30 W m^{-2}, typical solar UV power on a perfectly sunny day around noon, the real illumination time can be normalized ($t_{30W,n}$) using Eq. (5) [26]:

$$t_{30W,n} = t_{30W,n-1} + \Delta t_n \frac{\overline{UV_{G,n}}}{30} \frac{V_i}{V_T}; \quad \Delta t_n = t_n - t_{n-1}; \quad t_0$$
$$= 0 \, (n = 1) \quad (5)$$

where V_r is the total irradiated volume (24 L, glass tubes).

From Eqs. (3) and (5), the relationship between $Q_{UV,n}$ and $t_{30W,n}$ is

$$Q_{UV,n} = t_{30W,n} \frac{30 A_i}{V_i} \quad (6)$$

From Eq. (6), and according to the characteristics of the reactor, a $t_{30W,n}$ of 4.33 min is needed to accumulate 1 kJ L^{-1} of UV energy. Taking this value into account, the $t_{30W,n}$ necessary to reduce BPA concentration 50% ($t_{30W,BPA(50)}$) was found by multiplying it by $Q_{UV,BPA(50)}$ (Eq. (4)) (see Table 2). For the Fenton system (Run 18), k and $t_{BPA(50)}$ were obtained directly from Eq. (1).

The order of BPA degradation efficiency (higher k' and lower $t_{30W,BPA(50)}$) of the different oxidation systems under the experimental conditions in this study was as follows:

Photo-Fenton ~ Fenton > Fe(III)/oxalic pH 3 ~ Fe(III)/oxalic pH 6.5 > Fe(III)/citric pH 6.5 ~ TiO$_2$/Fe(III) pH 3 > TiO$_2$/Fe$_2$O$_3$ pH 3 ~ TiO$_2$/H$_2$O$_2$ pH 3 > TiO$_2$ pH 6.5 > TiO$_2$/Fe$_2$O$_3$ pH 6.5 > TiO$_2$ pH 3 > rest of systems. Systems in which the effect on BPA degradation was negligible are marked (ND) in Table 2.

As expected, the Fenton and photo-Fenton processes were the most effective systems, leading to similar BPA half-lives (1–2 min, see Table 2). While the Fenton system is able to generate HO$^{\bullet}$ radicals by Reaction (7), the presence of UV light (photo-Fenton) contributes to the formation of HO$^{\bullet}$ as well as to maintaining of Fe(II) in solution by Reaction (8):

$$Fe(II) + H_2O_2 \rightarrow Fe(III) + HO^{\bullet} + HO^- \quad (7)$$

$$Fe(OH)^{2+} \xrightarrow{h\nu} Fe(II) + HO^{\bullet} \quad (8)$$

In the photo-Fenton system HO$^{\bullet}$ radicals can also be formed by H$_2$O$_2$ photolysis:

$$H_2O_2 \xrightarrow{h\nu} 2HO^{\bullet} \quad (9)$$

However, although the quantum yield of H$_2$O$_2$ photolysis is high (~1 mol einstein^{-1} at wavelengths from 200 nm to 400 nm; [27] and references therein), photolysis scarcely takes place due to the low molar absorptivity of hydrogen peroxide at wavelengths > 320 nm ($\varepsilon_{H_2O_2} < 0.24$ M^{-1} cm^{-1} [28]). Thus the k' for BPA degradation by photolysis of H$_2$O$_2$ 10^{-3} M at pH 3 (Run 14) was low (0.093 L kJ^{-1}), and similar to that found by photolysis of Fe(III) 5 × 10^{-5} M at pH 3 by Reaction (8) (Run 2, k' = 0.089 L kJ^{-1}). In the absence of light H$_2$O$_2$ was not able to degrade BPA (not shown). Even though the quantum yield of Reaction (8) is lower than Reaction (9) (from 0.16 mol einstein^{-1} at 320 nm to 0.05 mol einstein^{-1} at 380 nm [29–31]), Fe(OH)$^{2+}$ molar absorp-

Table 2
Pseudo-first-order BPA rate constants, Q_{UV} and t_{30W} values for the reduction of BPA, total phenolic intermediates (PI) and TOC. Experimental conditions in Table 1.
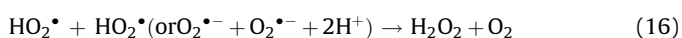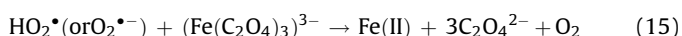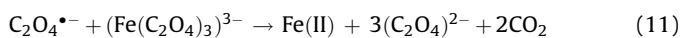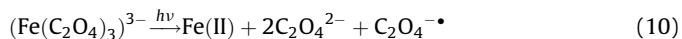
Run	System	k' L kJ^{-1}	R^2	$Q_{UV,BPA(50)}$ (kJ L^{-1})	$t_{30W,BPA(50)}$ (min)	$Q_{UV,PI(90)}$ (kJ L^{-1})	$t_{30W,PI(90)}$ (min)	$Q_{UV,TOC(15)}$ (kJ L^{-1})	$t_{30W-TOC(15)}$ (min)	$Q_{UV-TOC(50)}$ (kJ L^{-1})	$t_{30W-TOC(50)}$ (min)	$Q_{UV-TOC(75)}$ (kJ L^{-1})	$t_{30W-TOC(75)}$ (min)
1	UV$^{(ND)}$												
2	Fe(III) pH 3	0.089	0.962	7.74	34	>50	>200	39	169	≫50			
3	Fe(III) pH 6.5$^{(ND)}$												
4	Fe(III)/oxalic acid pH 3	1.349	0.991	0.51	2.2	38	165	7	30.2	44	192		
5	Fe(III)/oxalic acid pH 6.5	1.288	0.960	0.54	2.3	>50	>200			≫50			
6	Fe(III)/Citric acid pH 6.5	0.487	0.998	1.42	6.1	>50	>200			≫50			
7	TiO$_2$ pH 3	0.164	0.993	4.21	18	25	108	9	39.1	20.4	89	27.5	119
8	TiO$_2$ pH6.5	0.260	0.998	2.67	12	13	56	2.8	12.3	11.9	51	27.5	119
9	TiO$_2$/Fe(III) pH 3	0.430	0.999	1.61	7.0	13	56	4.5	19.2	11.0	48	17.4	75
10	α-Fe$_2$O$_3$ pH 3$^{(ND)}$												
11	α-Fe$_2$O$_3$ pH 6.5$^{(ND)}$												
12	TiO$_2$/α-Fe$_2$O$_3$ pH 3	0.319	0.998	2.17	9.4	18	78	5.7	24.7	15.0	82	21.2	92
13	TiO$_2$/H$_2$O$_2$ pH 3	0.312	0.999	2.22	9.6	23	99	9	39.1	18.4	79	26	112
14	H$_2$O$_2$ pH 3	0.093	0.996	7.44	32.2	>50	>200			≫50		–	–
15	TiO$_2$/α-Fe$_2$O$_3$ pH 6.5	0.211	0.997	3.29	14	13	56	4.5	19.2	10.5	45	14.4	62
16	α-Fe$_2$O$_3$/oxalic acid pH 6.5	0.049	0.996	14.1	61	>50	>200			≫50	–		–
17	Photo-Fenton pH 3	2.501	0.973	0.28	1.2	2.5	11	0.65	2.7	3.3	14.4	11	47
18	Fenton pH 3	(k = 0.345 min^{-1})^a	0.994		1.9^a		39^a		18^a		–	–	–

$^{(ND)}$ no or negligible degradation.
^{a} Determined directly from real reaction time.

tivity is higher (1535 M^{-1} cm^{-1} at 320, 560 M^{-1} cm^{-1} at 350 nm and 35 M^{-1} cm^{-1} at 400 nm [32]).

After the photo-Fenton and Fenton systems, the ferricarboxylate photolysis (Runs 4–6) systems were the most efficient for BPA removal. The ferrioxalate complex, which is undoubtedly the ferricomplex most studied, generates radicals with a quantum yield higher than that of Fe(III) itself. This complex photoreduces and decarboxylates in the presence of UVA–visible light with a quantum yield of 1.2 mol per photon, in terms of Fe(II) formation, at wavelengths between 250 nm and 450 nm [33,34] by Reactions (10)–(16) [35]:

$$(Fe(C_2O_4)_3)^{3-} \xrightarrow{h\nu} Fe(II) + 2C_2O_4{}^{2-} + C_2O_4{}^{-\bullet} \tag{10}$$

$$C_2O_4{}^{\bullet-} + (Fe(C_2O_4)_3)^{3-} \rightarrow Fe(II) + 3(C_2O_4)^{2-} + 2CO_2 \tag{11}$$

$$C_2O_4{}^{\bullet-} \rightarrow CO_2 + CO_2{}^{\bullet-} \tag{12}$$

$$CO_2{}^{\bullet-} + O_2 \rightarrow CO_2 + O_2{}^{\bullet-} \tag{13}$$

$$HO_2{}^\bullet \rightleftharpoons H^+ + O_2{}^{\bullet-} \quad pK_a = 4.8 \tag{14}$$

$$HO_2{}^\bullet(orO_2{}^{\bullet-}) + (Fe(C_2O_4)_3)^{3-} \rightarrow Fe(II) + 3C_2O_4{}^{2-} + O_2 \tag{15}$$

$$HO_2{}^\bullet + HO_2{}^\bullet(orO_2{}^{\bullet-} + O_2{}^{\bullet-} + 2H^+) \rightarrow H_2O_2 + O_2 \tag{16}$$

H_2O_2 generated by (16) can react with Fe(II) formed from (10), (11) and (15), leading to $HO^\bullet$ radicals by the Fenton reaction (Reaction (7)). Similar to ferrioxalate, citric acid also forms Fe(III) complexes (ferricitrate) that photoreduce in the presence of UVA–visible light and generate radical species [36,37]. Moreover, at pH 6.5, the presence of these carboxylates could on one hand, favour the maintenance of Fe(III) in solution by forming ferricomplexes and at least partially avoiding iron coagulation and precipitation [38]; and, on the other hand, the formation of H_2O_2 by promoting displacement of equilibrium (14) to superoxide radical ($O_2{}^{\bullet-}$) formation, which recombines to yield H_2O_2 through Reaction (16), that has a rate constant of $9.7\cdot10^7$ M^{-1} s^{-1} [35], which is 100 times higher than that of the hydroperoxide radical, $HO_2{}^\bullet$ (8.3×10^5 M^{-1} s^{-1} [35]).

In the TiO$_2$/UV system, radicals are generated by the following mechanism:

$$TiO_2 + h\nu \rightarrow TiO_2(e^-, h^+) \tag{17}$$

$$(h^+) + RX_{ad} \rightarrow RX_{ad}{}^{\bullet+} \tag{18}$$

$$(h^+) + H_2O_{ad} \rightarrow HO_{ad}{}^\bullet \tag{19}$$

$$(h^+) + HO_{ad}{}^- \rightarrow HO_{ad}{}^\bullet \tag{20}$$

$$(e^-) + O_2 \rightarrow O_2{}^{\bullet-} \tag{21}$$

$O_2{}^{\bullet-}$ radicals (and/or $HO_2{}^\bullet$ according to equilibrium (14)) could also recombine and generate H_2O_2 by (16). Hydrogen peroxide formed could, in turn, act as an electron acceptor generating hydroxyl radicals by (22):

$$(e^-) + H_2O_2 \rightarrow HO^\bullet + HO^- \tag{22}$$

Thus, organics in water could be oxidized by positive holes (Reaction (18)) and by $HO^\bullet$ radicals formed by (19), (20) and (22):

$$RX_{ad} + HO_{ad}{}^\bullet \rightarrow Products \tag{23}$$

$$RX + HO^\bullet \rightarrow Products \tag{24}$$

where RX_{ad} and RX mean any adsorbed or unadsorbed organic compound in water, respectively.

Aqueous pH has a dominating effect in photocatalytic reactions since it can affect the semiconductor surface, its band-gap and the ionization of organic contaminants. Thus, as observed in Fig. 1 and Table 2, BPA degradation level by TiO$_2$/UV at pH 6.5 (Run 8, k' 0.260 L kJ^{-1}) was higher than that observed at pH 3 (Run 7, k' 0.163 L kJ^{-1}), which could be related to the point of zero charge (PZC) of TiO$_2$ P25 (6.4 [39]) and the pK_a of BPA (9.6–10.2 [3]). Hence, at pH < 6.4, the TiO$_2$ surface is positively charged, and at pH > 6.4, it is negatively charged, while at pH < 9.7, BPA is mainly molecular. Then compared to pH 3, at pH 6.5 electrostatic interactions between BPA and the TiO$_2$ surface are favoured.

Moreover, generation of free hydroxyl radicals from the photooxidation of HO^- by holes on the TiO$_2$ surface (Reaction (20)) increases with pH, as well as the H_2O_2 generation rate by Reaction (16). Similar results were found by Kaneco et al. when degrading BPA with a TiO$_2$/solar light system [11].

The positive effect of dissolved Fe(III) on the TiO$_2$/UV system efficiency by acting as an electron acceptor similar to O_2 (Reaction (21)) and H_2O_2 (Reaction (22)), and avoiding e^-–h^+ recombination by (25), has been reported in the literature [36,37,40,41].

$$(e^-) + Fe(III) \rightarrow Fe(II) \tag{25}$$

The synergistic effect of Fe(III) at low pH (Run 9) is shown clearly in Fig. 1 and Table 2. Thus, while $t_{30W,BPA(50)}$ for the Fe(III)/UV system at pH 3 (Run 2) and the TiO$_2$/UV system at pH 3 (Run 7) was 34 and 18 min, respectively, for the TiO$_2$/Fe(III)/UV system at pH 3 (Run 9) it was less than 7 min, which is also less than that needed by the TiO$_2$/H$_2$O$_2$/UV system at pH 3 (Run 13, 9.6 min) and by the TiO$_2$/UV system at pH 6.5 (Run 8, 12 min).

Several studies have confirmed the positive effect of iron (III) oxides on the efficiency of the TiO$_2$/UV system, similar to dissolved Fe(III) ([38,42–44]). Thus, as seen in Fig. 1 and Table 2 for the experimental conditions applied in this study, $t_{30W,BPA(50)}$ for the TiO$_2$/α-Fe$_2$O$_3$/UV system at pH 3 (Run 12) was 9.4 min, shorter than that for the TiO$_2$/UV system at pH 3 (18 min, Run 7), and similar to that of the TiO$_2$/H$_2$O$_2$/UV system at pH 3 (9.6 min, Run 13). However, at pH 6.5, the presence of α-Fe$_2$O$_3$ seems to exert a negative effect on BPA degradation, since for the TiO$_2$/α-Fe$_2$O$_3$/UV system at pH 6.5 (Run 15), $t_{30W,BPA(50)}$ was 14 min, slightly higher than that observed with the TiO$_2$/UV system at pH 6.5 (12 min, Run 8).

The effect of the presence of α-Fe$_2$O$_3$ on the efficiency of TiO$_2$/UV depends on factors such as the photocatalytic activity of α-Fe$_2$O$_3$ (positive), its interaction with the TiO$_2$ surface by lowering its band-gap and/or by acting as an e^- acceptor (positive), its dissolution (positive since dissolved Fe(III) could act by (8), and/or (10)–(16) and/or (25), depending on the media), and the reduction of the radiation path through the solution (negative), and so forth.

According to the results found in a previous study [38], and as deduced from Table 2, the α-Fe$_2$O$_3$ applied here did not show any photocatalytic activity (see Runs 10 and 11 at pH 3 and 6.5, respectively). On the other hand, Fe(III) complexing agents (oxalic, citric, tartaric, malonic, etc.), as well as the TiO$_2$/UV system, promote iron (III) oxide dissolution, and the leaching process is more pronounced under acidic conditions [38]. Hence, as observed in Fig. 2, where total dissolved Fe concentration ([Fe$_T$]) is plotted as a function of $Q_{UV,n}$, TiO$_2$/UV favoured α-Fe$_2$O$_3$ dissolution at pH 3, and a maximum [Fe$_T$] of about 5×10^{-5} M was attained with a Q_{UV} of 25 kJ L^{-1}. On the contrary, at pH 6.5 maximum [Fe$_T$] was 10 times lower than that at pH 3, either because α-Fe$_2$O$_3$ dissolution was negligible at pH 6.5, or because dissolved Fe, if formed, would precipitate as iron hydroxide. If Fe remains in solution as Fe(III), it can lead to $HO^\bullet$ radical formation by (8) and/or increase TiO$_2$ efficiency by (25), thus explaining the good results obtained in BPA degradation by the TiO$_2$/α-Fe$_2$O$_3$/UV system at pH 3.
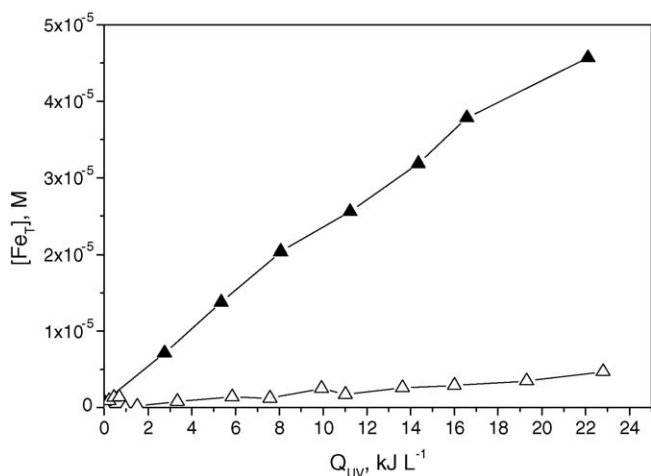
Fig. 2. Iron leaching from α-Fe$_2$O$_3$ in the presence of TiO$_2$ during reaction time. Influence of pH. Experimental conditions in Table 1. Symbols: ▲, TiO$_2$/α-Fe$_2$O$_3$/UV pH 3 (Run 12); △, TiO$_2$/α-Fe$_2$O$_3$/UV pH 6.5 (Run 15).

As mentioned above, the presence of Fe(III) complexing agents, such as oxalic acid, could enhance α-Fe$_2$O$_3$ dissolution by an adsorption–complexation–dissolution mechanism [45]. Ferrioxalate formed could then, in addition, photoreduce and generate radical species by (10)–(16) when exposed to UV–vis light. Although dissolution is enhanced in acidic conditions, α-Fe$_2$O$_3$ can also be partly dissolved in the presence of oxalic acid at higher pH [38]. Thus, as seen in Table 2 and Fig. 1, $t_{30W,BPA(50)}$ for α-Fe$_2$O$_3$/oxalic acid/UV system at pH 6.5 (Run 16) was 61 min, when [Fe$_T$] was 5×10^{-6} M, which is similar to the TiO$_2$/α-Fe$_2$O$_3$/UV system at pH 6.5 (Run 15, $t_{30W,BPA(50)}$ 14 min).

3.2. Degradation of phenolic intermediates

Some authors have postulated that the first intermediates formed during BPA degradation are more toxic than the parent compound itself [10]. It is therefore of interest to find out how total phenolic intermediates (PIs) evolve during application of the different degradation processes. In Fig. 3 the PI evolution (expressed as BPA equivalents) with accumulated UV energy in the reactor (Q_{UV}) is shown for different systems. The UV radiation
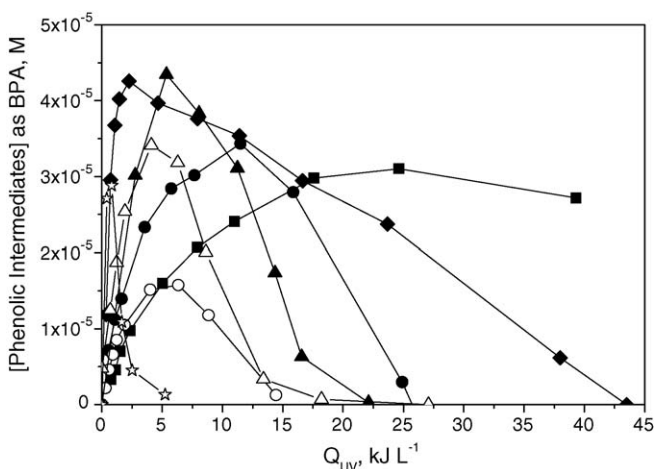
Fig. 3. Evolution of phenolic intermediates concentration (expressed as BPA equivalents) with accumulated UV energy. Experimental conditions in Table 1. Symbols: ■, Fe(III)/UV pH 3 (Run 2); ◆, Fe(III)/oxalic acid/UV pH 3 (Run 4); ●, TiO$_2$/UV pH 3 (Run 7); ○, TiO$_2$/UV pH 6.5 (Run 8); △, TiO$_2$/Fe(III) pH 3 (Run 9); ▲, TiO$_2$/α-Fe$_2$O$_3$/UV pH 3 (Run 12); ☆ Fe(II)/H$_2$O$_2$/UV pH 3 (Run 17).

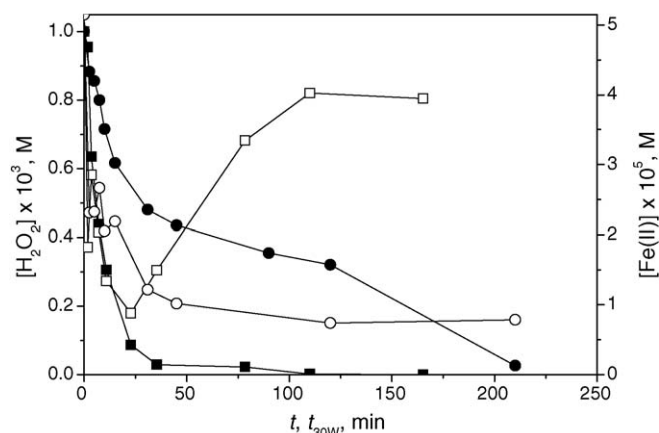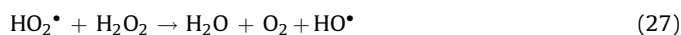**Fig. 4.** Evolution of H$_2$O$_2$ (solid symbols) and Fe(II) (open symbols) concentration with time. Experimental conditions in Table 1. Symbols: ■, □ Fe(II)/H$_2$O$_2$/UV (Run 17); ●, ○ Fe(II)/H$_2$O$_2$ (Run 18).

needed to achieve a 90% reduction in PI ($Q_{UV,PI(90)}$), which implies a phenolic intermediates concentration of 5×10^{-6} M expressed as BPA equivalents, was determined from these results, as shown in Table 2. In addition to $Q_{UV,PI(90)}$ data, $t_{30W,PI(90)}$ was calculated for each experiment according to Eq. (6) (see Table 2). For the Fenton system (Run 18), the time needed to reach this PI concentration was determined directly from the experiment time.

As shown in Table 2, the order of efficiency of the different systems in reducing phenol content was:

Photo-Fenton > Fenton > TiO$_2$ pH 6.5 ~ TiO$_2$/α-Fe$_2$O$_3$ pH 6.5 ~ TiO$_2$/Fe(III) pH 3 > TiO$_2$/α-Fe$_2$O$_3$ pH 3 > TiO$_2$/H$_2$O$_2$ pH 3 > TiO$_2$ pH 3 > Fe(III)/oxalic acid pH 3 ≫ other systems.

Again, photo-Fenton and Fenton were the most effective systems of all those tested. However, although there was barely a difference in $t_{30W,BPA(50)}$ and $t_{BPA(50)}$ (1–2 min), $t_{30W,PI(90)}$ and $t_{PI(90)}$ values were very different, being 11 min for the photo-Fenton system (Run 17) and 39 min for the Fenton system (run 18). The explanation for these results can be inferred from Fig. 4, which shows the evolution of H$_2$O$_2$ and Fe(II) concentrations with (t_{30W} and t). The higher efficiency of the photo-Fenton process is likely due to Reaction (8), which contributes to the formation of HO$^\bullet$ radicals as well as to maintaining Fe(II) in solution, which reacts with H$_2$O$_2$, generating HO$^\bullet$ (Reaction (7)). Once H$_2$O$_2$ is depleted in the presence of UV light (t_{30W} = 34 min, Fig. 4), Reaction (8) is the main source of radicals. On the contrary, in absence of light, Fe(II) is oxidized almost completely to Fe(III) by (7), and after 50 min, only 20% of the total dissolved iron is Fe(II) (see Fig. 4), thus resulting in a lower HO$^\bullet$ production rate. Although H$_2$O$_2$ can reduce Fe(III) to Fe(II) by Reaction (26) and generate HO$^\bullet$ radicals by (27), the rate constant of Reaction (26) is very low compared to Reaction (7) (0.002 M^{-1} s^{-1} and 75 M^{-1} s^{-1}, respectively [46,47]).

$$Fe^{3+} + H_2O_2 \rightarrow Fe^{2+} + H^+HO_2^\bullet \tag{26}$$

$$HO_2^\bullet + H_2O_2 \rightarrow H_2O + O_2 + HO^\bullet \tag{27}$$

As observed in BPA degradation, the PI elimination rate in the TiO$_2$/UV system increased with pH ($t_{30W,PI(90)}$ of 108 min and 56 min at pH 3 and 6.5, respectively), which again would be related to a better interaction between the surface of the catalyst and the intermediates formed at higher pH. There is also a synergistic effect between Fe(III) (in solution or as oxide) and TiO$_2$/UV on PI degradation by the mechanisms mentioned in Section 3.1. For instance, while $t_{30W,PI(90)}$ was higher than 200 min and 108 min in the Fe(III)/UV and TiO$_2$/UV systems, respectively, this time was shortened to 56 min and 78 min in the TiO$_2$/Fe(III)/UV and TiO$_2$/α-
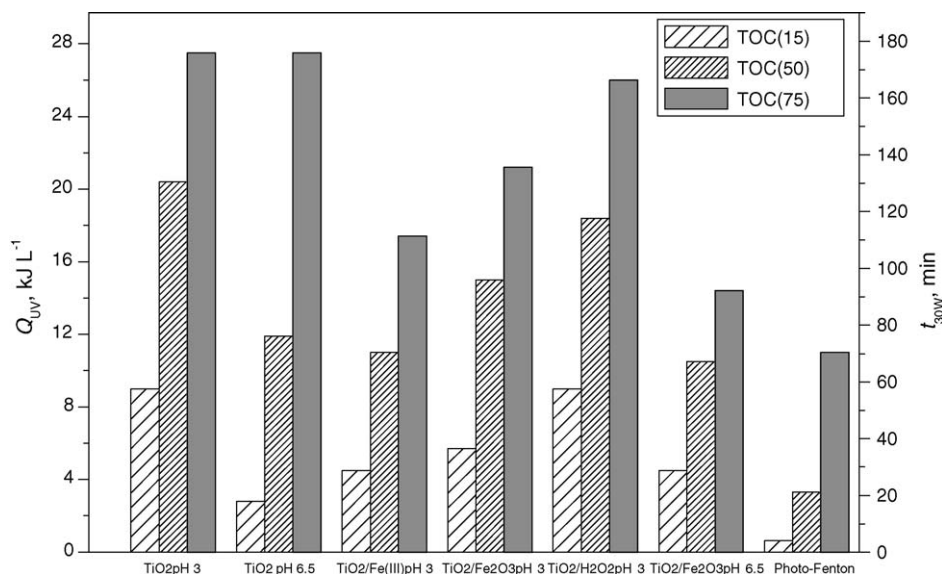
Fig. 5. Accumulated UV energy (Q_{UV}) and t_{30W} needed for the reduction of 15%, 50% and 75% of initial TOC content. Experimental conditions in Table 1.

Fe$_2$O$_3$/UV systems at pH 3, respectively. Moreover, while at pH 6.5, α-Fe$_2$O$_3$ exerted a slightly negative effect on BPA degradation by the TiO$_2$/UV system, its effect on PI elimination was negligible.

Examining the order of PI degradation efficiency in comparison to BPA degradation, systems based on ferricarboxylate photolysis turned out to be less effective in eliminating PIs. In the Fe(III)/oxalic acid/UV system at pH 3 (Run 4) the loss of efficiency might derive from rapid mineralization of oxalic acid by Reactions (10)–(16). Thus, once oxalic acid was completely depleted (which happened at t_{30W} = 20 min; not shown), only Reaction (8) generates HO$^\bullet$ radicals until complete photoreduction of Fe(III) to Fe(II). In the systems that applied oxalic acid at pH 6.5 (Runs 5 and 16), only 20% of oxalic acid was mineralized (not shown), so the loss of efficiency could be attributed to a lower concentration of ferrioxalate in the media due to Fe(III) coagulation at this pH.

3.3. Mineralization

Another important aspect of AOP application is their mineralization affiance. To compare the efficiency of the different systems tested, and taking into account the mineralization of oxalic acid in the runs it was added to (Runs 4, 5, and 16), the percentage of TOC mineralized (from BPA) was plotted against Q_{UV}. From these plots, the Q_{UV} required by the different AOPs for 15%, 50% and 75% TOC mineralization ($Q_{UV,TOC(15)}$, $Q_{UV,TOC(50)}$ and $Q_{UV,TOC(75)}$, respectively) was found as summarized in Table 2 along with the t_{30W} (found from Q_{UV} using Eq. (6)) needed to reach them ($t_{30W,TOC(15)}$, $t_{30W,TOC(50)}$ and $t_{30W,TOC(75)}$). The actual experimental time is given for the Fenton system.

As shown in Table 2, the time needed to reach 75% of TOC mineralization increases in the following order:

Photo-Fenton > TiO$_2$/α-Fe$_2$O$_3$ pH 6.5 > TiO$_2$/Fe(III) pH 3 > TiO$_2$/α-Fe$_2$O$_3$ pH 3 > TiO$_2$/H$_2$O$_2$ pH 3 ∼ TiO$_2$ pH 3 ∼ TiO$_2$ pH 6.5 ≫ other systems.

If this sequence is compared to the order found for BPA and PI degradation, the Fenton system is observed to lose efficiency regarding mineralization, which would be attributable, as discussed in Section 3.2, to the low Fe(II) concentration remaining in solution (see Fig. 4). Thus, when H$_2$O$_2$ was completely depleted (t = 210 min), mineralization was only 30%.

Of the systems tested, the photo-Fenton was clearly superior form the point of view of mineralization as deduced from Fig. 5, where the Q_{UV} and t_{30W} required to mineralize 15%, 50% and 75% of

TOC are shown for the most effective systems. Thus, during photo-Fenton, mineralization took place even when the H$_2$O$_2$ had been exhausted (t_{30W} = 34 min, Fig. 4) due to the contribution of Reaction (8) to HO$^\bullet$ formation, and probably also to the formation of carboxylates able to form photoactive ferricomplexes (malic, tartaric, oxalic, etc.) and hence, their photodegradation, since these acids were not detected by ionic chromatography during this run.

As shown in Fig. 5, the initial mineralization rate observed with the TiO$_2$/UV system at pH 6.5 was higher than those observed for the rest of the runs this catalyst was used in. However, its efficiency gradually diminished, and the $t_{30W,TOC(75)}$ was the same as for the TiO$_2$/UV system at pH 3 (119 min in both cases). Moreover, regardless of the working pH, the TiO$_2$/UV system mineralization efficiency was improved by the presence of Fe(III) or α-Fe$_2$O$_3$. Thus, for TiO$_2$/α-Fe$_2$O$_3$ at pH 6.5 (Run 15), TiO$_2$/Fe(III) at pH 3 (Run 9) and TiO$_2$/α-Fe$_2$O$_3$ at pH 3 (Run 12), $t_{30W,TOC(75)}$ was 62, 75 and 92 min, respectively.

Although, as mentioned in the sections above, at pH 6.5 the BPA and PI degradation rates by the TiO$_2$/UV system were higher than
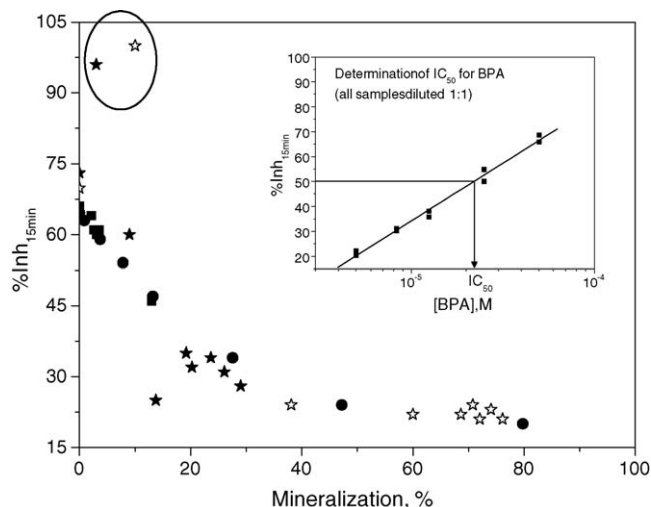

Fig. 6. Evolution of toxicity with mineralization for different AOPs. Experimental conditions in Table 1. Symbols: ■, Fe(III)/UV pH 3 (Run 2); ●, TiO$_2$/UV pH 3 (Run 7); ☆, Fe(II)/H$_2$O$_2$/UV pH 3 (Run 17); ★, Fe(II)/H$_2$O$_2$ pH 3 (Run 18). Insert graph: determination of IC$_{50}$ for BPA. In all cases, samples were diluted 1:1 before the analysis.

at pH 3, the mineralization results were poorer, which could indicate the formation of low-weight carboxylic acids which at pH 6.5 would be ionic, thus impeding their interaction with the catalyst surface. This is the case of muconic and oxalic acids, intermediates of phenol oxidation [48–50], which in their ionic form (muconate and oxalate) are poorly oxidized by TiO_2/UV [37,51,52]. Also, this reasoning could explain the $t_{30W,TOC(75)}$ in the TiO_2/UV system at pH 3 and 6.5 (119 min in both cases).

On the other hand, improvement of TiO_2/UV mineralization efficiency by the presence of Fe(III) (either dissolved or as an oxide) would be at least partly attributable to the formation of photoactive ferricarboxylates (ferrimalate, ferritartrate, ferrioxalate, etc.) that would generate (the same as observed in Runs 4–6 and 16) radical species during their photoreduction, thus
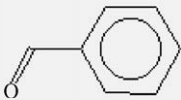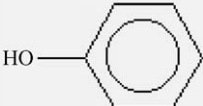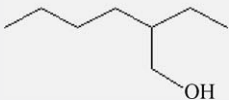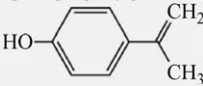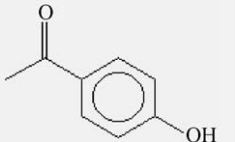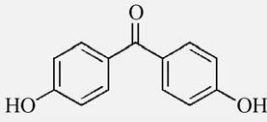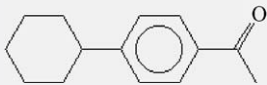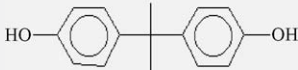
contributing not only to their own degradation, but also to the degradation of other intermediates present.

As shown in Table 2 and Fig. 5, the presence of H_2O_2 improved the mineralization efficiency of the TiO_2/UV system at pH 3 only slightly. Since all H_2O_2 was consumed during this Run, from the point of view of process economy, the combination TiO_2/H_2O_2/UV at pH 3 is not of interest.

3.4. Toxicity

Toxicity during the different AOPs was studied by measuring the luminescence inhibition of the marine bacterium V. fischeri. The results are shown in Fig. 6, where the percentage inhibition after 15 min is plotted as a function of mineralization for the Fe(III)/UV,

Table 3
BPA byproducts detected by GC–MS.

| Compound	Substance	Formula	CAS	Ion	t_R (min)	NIST quality (%)
1	Benzaldehyde	C_7H_6O	100-52-7	51(35) 77(77) 105(100) 106(86)	4.470	93
2	Phenol	C_6H_6O	108-95-2	66 (42) 94(100)	4.504	92
3	1-Hexanol-2-ethyl	$C_8H_{18}O$	104-76-7	57(100) 70(23) 83(27)	4.663	85
4	p-isopropenylphenol	$C_9H_{10}O$	4286-23-1	91(27) 119(77) 134(100)	7.012	93
5	Acetophenone, 4'-hydroxy	$C_8H_8O_2$	99-93-4	65(20) 93(31) 121(100) 136(32)	8.543	97
6	4,4'-dihydroxybenzophenone	$C_{13}H_{10}O_3$	611-99-4	77(89) 121(83) 214(100)	12.304	85
7	Ethanone, 1-(4-cyclohexylphenyl)	$C_{14}H_{18}O$	18594-05-3	187(100) 202(25)	15.568	81
8	4,4´-isopropylidenediphenol (BPA)	$C_{15}H_{16}O_2$	80-05-7	213(100)	15.916	99
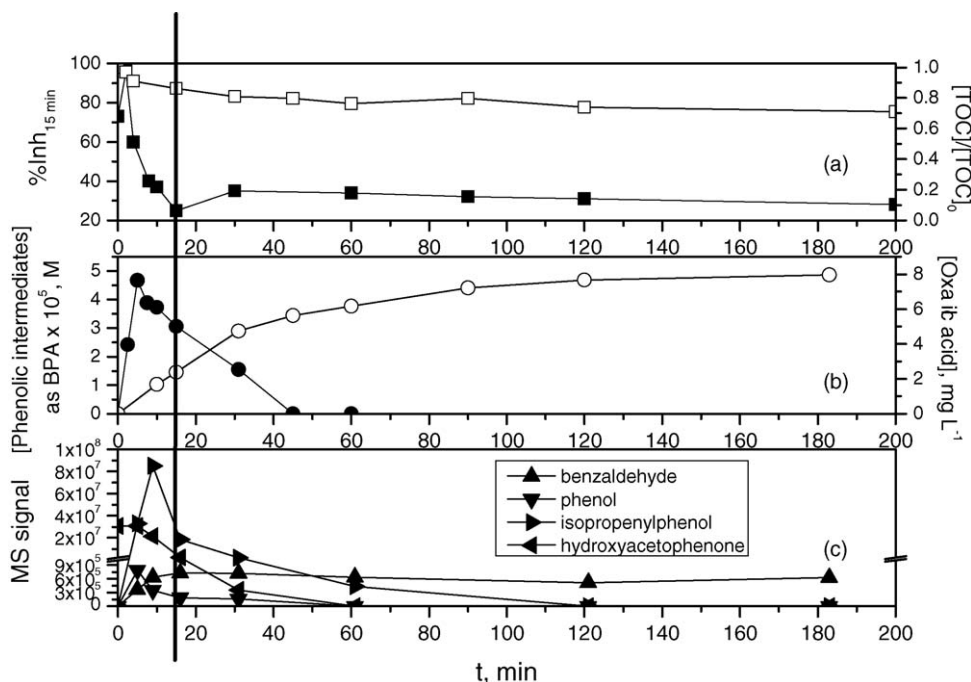
Fig. 7. Evolution of different contamination parameters with time for the Fenton system (Run 18). Symbols: (a) □, TOC; ■, toxicity; (b) ○, [oxalic acid]; ●, total phenolic intermediates (Folin-Ciocalteau method); (c) ▲, ▼, ▶, ◀, Aromatic intermediates identified by GC–MS.

TiO$_2$/UV, Fenton and photo-Fenton systems (all of them at pH 3). The IC$_{50}$ (BPA concentration causing a 50% reduction in luminescence) after 15 min is 2.2×10^{-5} M (5 mg L^{-1}), as shown in Fig. 6. Since all samples (including standards) were diluted 1:1 before analysis, the IC$_{50}$ is 2.5 mg L^{-1}.

As observed in Fig. 6, regardless of the process tested, there is an obvious relationship between TOC conversion and toxicity. Toxicity diminished from 70% to 30% when mineralization was 20%. However, there was an increase in toxicity at the beginning of the Fenton and photo-Fenton runs. According to the literature, this increase could be related to the formation and accumulation of reaction intermediates that would be more toxic than BPA [10], as discussed in the following section.

3.5. GC/MS identification of intermediates

The nature and evolution over time of the intermediates generated during BPA oxidation by Fenton system (Run 18) were also studied. Table 3 summarizes the main fragments (m/z), retention times (t_R) and relative abundance (%) for the identified intermediate products, some of them phenolic such as phenol, p-isopropenylphenol and 4-hydroxyacetophenone, among others. These intermediates have also been identified by other authors during BPA oxidation by AOPs [11,13,17]. According to Fig. 7, where the different contamination parameters are plotted over the reaction time in Run 18, there seems to be a relationship between the amount of phenol intermediates generated and the toxicity of the sample. Thus, the increase in toxicity observed at the beginning of the reaction corresponds to the accumulation of PIs (determined by the Folin-Ciocalteau method and by GC–MS), and toxicity diminishes as these intermediates disappear. According to these results, the PI concentration as determined by the Folin-Ciocalteau method could also be considered an indicative parameter of sample toxicity.

4. Conclusions

Under the experimental conditions in this study, at pH 3 Fenton and photo-Fenton systems 3 were the most effective in BPA and PI

degradation. At this pH the most mineralization was achieved by photo-Fenton and TiO$_2$/Fe(III) systems. At pH 6.5, the highest BPA degradation rate was found for the Fe(III)/oxalic acid, and the TiO$_2$/UV system (either in absence or presence of α-Fe$_2$O$_3$) was the most effective in PI oxidation, and α-Fe$_2$O$_3$ exerted a positive effect mainly on mineralization.

There is a strong relationship between mineralization and toxicity. The results also indicate that some of the phenolic intermediates formed could be more toxic than BPA.

References

[1] J. Xu, Y. Osuga, T. Yano, Y. Morita, X. Tang, T. Fujiwara, Y. Takai, H. Matsumi, K. Koga, Y. Taketani, O. Tsutsumi, Biochem. Biophys. Res. Commun. 292 (2002) 456.
[2] H. Iida, K. Maehara, M. Doiguchi, T. Mori, F. Yamada, Reprod. Toxicol. 17 (2003) 457–468.
[3] C. Staples, P.B. Dome, G.M. Klecka, S.T. Oblock, L.R. Harris, Chemosphere 36 (1998) 2149–2173.
[4] S.Y. Park, J. Choi, Environ. Int. 33 (2007) 817–822.
[5] E.M. Mihaich, U. Friederich, N. Caspers, A.T. Hall, G.M. Klecka, S.S. Dimond, C.A. Staples, L.S. Ortego, S.G. Hentges, Ecotoxicol. Environ. Saf. 72 (2009) 1392–1399.
[6] J. Zhao, Y. Li, C. Zhang, Q. Zeng, Q. Zhou, J. Hazard. Mater. 155 (2008) 305–311.
[7] H. Gallard, A. Leclercq, J.P. Croué, Chemosphere 56 (2004) 465–473.
[8] N. Nakada, H. Shinohara, A. Murata, K. Kiri, S. Managaki, N. Sato, H. Takada, Water Res. 41 (2007) 4373–4382.
[9] I. Gültekin, N.H. Ince, J. Environ. Manage. 85 (2007) 816–832.
[10] K. Chiang, T.M. Lim, L. Tsen, C.C. Lee, Appl. Catal. A: Gen. 261 (2004) 225–237.
[11] S. Kaneco, M.A. Rahman, T. Suziki, H. Katsumata, K. Ohta, J. Photochem. Photobiol. A: Chem. 163 (2004) 419–424.
[12] P. Chen, K.G. Linden, D.E. Hinton, S. Kawashida, E.J. Rosenfeldt, S.W. Kullman, Chemosphere 65 (2006) 1094–1102.
[13] H. Katsumata, S. Kawabe, S. Kaneco, T. Suzuki, K. Ohta, J. Photochem. Photobiol. A: Chem. 162 (2004) 297–305.
[14] Z. Peng, F. Wu, N. Deng, Environ. Pollut. 144 (2006) 840–846.
[15] M. Zhan, X. Yang, Q. Xian, L. Kong, Chemosphere 63 (2006) 378–386.
[16] D. Zhou, F. Wu, N. Deng, W. Xiang, Water Res. 38 (2004) 4107–4116.

[17] R.A. Torres, C. Pétrier, E. Combet, M. Carrier, C. Pulgarín, Ultrason. Sonochem. 15 (2008) 605–611.
[18] M. Lapertot, C. Pulgarin, P. Fernández-Ibáñez, M.I. Maldonado, L. Pérez-Estrada, I. Oller, W. Gernjak, S. Malato, Water Res. 40 (2006) 1086–1094.
[19] L.L. Stookey, Anal. Chem. 42 (1970) 779–781.
[20] E.M. Rodríguez, M. Mimbrero, F.J. Masa, F.J. Beltrán, Water Res. 41 (2007) 1325–1333.
[21] Y. Zuo, Geochim. Cosmochim. Acta 59 (1995) 3123–3130.
[22] V.L. Singleton, J.A. Rossi, Am. J. Enol. Viticult. 16 (1965) 144–158.
[23] R.F.P. Nogueira, M.C. Oliveira, W.C. Paterlini, Talanta 66 (2005) 86–91.
[24] N. N. Klamerth, W. Gernjak, S. Malato, A. Agüera, B. B. Lendl, Water Res. 43 (2009) 441–449.
[25] J.P.V. Vilar, A.I.E. Gomes, V.M. Ramos, M.I. Maldonado, R.A.R. Boaventura, Photochem. Photobiol. Sci. 8 (2009) 691–698.
[26] A. Zapata, I. Oller, E. Bizani, J.A. Sánchez-Pérez, M.I. Maldonado, S. Malato, Catal. Today 144 (2009) 94–99.
[27] S. Goldstein, D. Aschengrau, Y. Diamant, J. Rabani, Environ. Sci. Technol. 41 (2007) 7486–7490.
[28] L. Chu, C. Anastasio, J. Phys. Chem. A 109 (2005) 6264–6271.
[29] H.J. Benkelberg, P. Warneck, J. Phys. Chem. 99 (1995) 5214–5221.
[30] P. Mazellier, J. Jirkovsky, M. Bolte, Pestic. Sci. 49 (1997) 259–267.
[31] C. Lee, J. Yoon, Chemosphere 57 (2004) 1449–1458.
[32] B.C. Faust, J. Hoigné, Atmos. Environ. 24A (1990) 79–89.
[33] V. Balzani, V. Carassiti, Photochemistry of Coordination Compounds, Academic Press, London, 1970.
[34] S. Goldstein, J. Rabani, J. Photochem. Photobiol. A: Chem. 193 (2008) 50–55.
[35] J. Jeong, J. Yoon, Water Res. 38 (2004) 3531–3540.
[36] N. Quici, M.E. Morgada, R.T. Gettar, M. Bolte, M. Litter, Appl. Catal. B: Environ. 71 (2007) 117–124.
[37] E.M. Rodríguez, B. Núñez, G. Fernández, F.J. Beltrán, Appl. Catal. B: Environ. 89 (2009) 214–222.
[38] E.M. Rodríguez, G. Fernández, B. Ledesma, P.M. Álvarez, F.J. Beltrán, Appl. Catal. B: Environ. 92 (2009) 240–249.
[39] M. Kosmulski, Adv. Colloid Interface 152 (2009) 14–25.
[40] H. Měšťánková, G. Mailhot, J. Jirkovský, J. Krýsa, M. Bolte, Appl. Catal. B: Environ. 57 (2005) 257–265.
[41] A.G. Rincón, C. Pulgarin, Appl. Catal. B: Environ. 63 (2006) 222–231.
[42] B. Tryba, A.W. Morawski, M. Inagaki, M. Toyoda, J. Photochem. Photobiol. A: Chem. 179 (2006) 224–228.
[43] B. Tryba, M. Piszcz, B. Grzmil, A. Pattek-Janczyk, A.W. Morawski, J. Hazard. Mater. 162 (2009) 111–119.
[44] F. Mazille, T. Schoettl, C. Pulgarín, Appl. Catal. B: Environ. 89 (2009) 635–644.
[45] R.M. Cornell, U. Schwertmann, The Iron Oxides: Structure, Properties, Reactions, Occurrences and Uses, 2nd edition, Wiley-VCH Verlag GmbH & Co. KGaA, Weinheim, 2003.
[46] J.J. Pignatello, Environ. Sci. Technol. 26 (1992) 944–951.
[47] D.A. Wink, R.W. Nims, M.F. Desrosiers, P.C. Ford, L.K. Keefer, Chem. Res. Toxicol. 4 (1991) 510–512.
[48] C.K. Scheck, F.H. Frimmel, Water Res. 29 (1995) 2346–2352.
[49] J. Chen, L. Eberlein, C.H. Langford, J. Photochem. Photobiol. A: Chem. 148 (2002) 183–189.
[50] J.A. Zazo, J.A. Casas, A.F. Mohedano, M.A. Gilarranz, J.J. Rodríguez, Environ. Sci. Technol. 39 (2005) 9295–9302.
[51] M.I. Franch, J.A. Ayllón, J. Peral, X. Doménech, Catal. Today 76 (2002) 221–233.
[52] C. Karunakaran, R. Dhanalakshmi, Sol. Energy Mater. Sol. Cells 92 (2008) 588–593.